Endocytic Selective Toxicity of Rhodamine 6G nanoGUMBOS in Breast Cancer Cells

Article *in* Molecular Pharmaceutics · July 2018

DOI: 10.1021/acs.molpharmaceut.8b00339

CITATIONS
12

READS
164

9 authors, including:

Nimisha Bhattarai
Tulane University
12 PUBLICATIONS **142** CITATIONS
SEE PROFILE

Mi Chen
Louisiana State University
8 PUBLICATIONS **74** CITATIONS
SEE PROFILE

Rocío Pérez
Georgia Southern University
30 PUBLICATIONS **419** CITATIONS
SEE PROFILE

Article

Endocytic Selective Toxicity of Rhodamine 6G nanoGUMBOS in Breast Cancer Cells

Nimisha Bhattarai, J. Michael Mathis, Mi Chen, Rocio L Perez, Noureen Siraj, Paul K.S. Magut, Karen McDonough, Girija Sahasrabudhe, and Isiah M Warner

Mol. Pharmaceutics, **Just Accepted Manuscript** • DOI: 10.1021/acs.molpharmaceut.8b00339 • Publication Date (Web): 05 Jul 2018

Endocytic Selective Toxicity of Rhodamine 6G nanoGUMBOS in Breast Cancer Cells

Nimisha Bhattarai,[a] J. Michael Mathis,[b] Mi Chen,[a] Rocío L. Pérez,[a] Noureen Siraj,[a,1] Paul K. S. Magut,[a,2] Karen McDonough,[c] Girija Sahasrabudhe,[a] and Isiah M. Warner [a*]

[a]Department of Chemistry, Louisiana State University, Baton Rouge, LA 70803, USA

[b]Department of Comparative Biomedical Sciences, School of Veterinary Medicine, Louisiana State University, Baton Rouge, LA 70803, USA

[c]AgCenter Biotechnology Labs, Louisiana State University, Baton Rouge, LA 70803, USA.

[1] Present address - Department of Chemistry, University of Arkansas at Little Rock, Little Rock, AR 72204, USA.

[2] Present address - Department of Chemistry, Dedan Kimathi University of Technology, Nyeri-Kenya

* Corresponding Author: Isiah M. Warner, email: iwarner@lsu.edu, Phone: 225-578-2829, Fax: 225-578-3971

Funding: This work was supported by the National Science Foundation (Grant No. CHE-1508726)

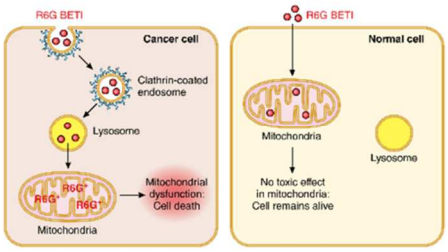

Graphical Abstract

Abstract

Herein, we report on the role of endocytosis in the selective chemotherpeutic toxicity of Rhodamine 6G (R6G) based nanomaterials, i.e. nanoGUMBOS, that are derived from a Group of Uniform Materials Based on Organic Salts (GUMBOS). Evaluation of cellular uptake in the presence and absence of endocytosis inhibitors suggests nanoGUMBOS internalization via clathrin-mediated endocytosis in cancer cells and reveals lack of endocytic internalization in normal cells. Results from characterization of these nanomaterials suggest that endocytic internalization in cancer cells leads to nanoGUMBOS dissociation within the endosomal environment. This ultimately results in selective cytotoxicity of the nanoGUMBOS for cancer cells with no toxicity towards normal cells under examined conditions. Following examination of the selectivity mechanism, *in vivo* investigations were performed to examine potential therapeutic properties of these nanoparticles. Remarkably, nanoGUMBOS treatment using a mouse xenograft model reduced the tumor volume by 50% suggesting retention of *in vitro* therapeutic properties *in vivo*. These results corroborate the selective behavior of nanoGUMBOS and demonstrate their *in vivo* therapeutic effects, providing further insight into the possible use of these nanomaterials as potential chemotherapeutic agents.

Keywords

Breast cancer; chemotherapy; Group of Uniform Materials Based on Organic Salts (GUMBOS); nanoGUMBOS; nanomaterials; Rhodamine 6G

Introduction

Despite development of several therapies, cancer remains the second most significant cause of death in the United States as of 2017.[1] Additionally, development of more targeted therapies has become essential due to detrimental side effects of conventional chemotherapeutic treatments. In this regard, nanomaterials have been extensively investigated for selective chemotherapeutic applications.[2-5] Conventional nanomedicines employed for chemotherapy typically focus on the use of nanoparticles comprised of polymers, quantum dots, silica and carbon nanotubes as drug carriers.[6-8] In contrast to conventional chemotherapy, these nanoscale delivery systems provide protection of the drug from biodegradation as well as nanoscale size for enhanced cellular uptake. [3, 6-7, 9] Furthermore, the tunable size, surface chemistry and shape of these nanomaterials can be exploited to alter their internalization pathway and ultimately their therapeutic properties.

Cellular uptake of nanoparticles typically occurs through active transport pathways, the most common of which is endocytosis.[10-18] Endocytosis can occur via two primary mechanisms: phagocytosis and pinocytosis. Phagocytosis is generally associated with the uptake of large particles (2-3 μm), while pinocytosis is associated with nanoscale particles. Pinocytosis is further divided into three categories 1) caveolin-mediated endocytosis, 2) clathrin-mediated endocytosis, and 3) macropinocytosis.[10-11] In the latter two pathways of pinocytosis, the vesicle encapsulating the particles forms an acidic endosome which later fuses with the lysosome. The contents of the endosome are metabolized and then released for subcellular localization. In contrast, in caveolin-mediated endocytosis, the vesicle typically bypasses the lysosome, preventing degradation of the particles due to the lysosomal environment comprised of acidic pH value and various enzymes.[10] Thus, the internalization pathway employed for nanomaterials can significantly alter their therapeutic properties. Several studies examining the selective chemotherapeutic toxicity of

nanomaterials have attributed their selective behavior to either targeting agents conjugated at the surface of nanomaterials or the pathway employed for cellular internalization.[15, 19] In regards to the latter, the overexpression of certain endocytic proteins on cancer cells can be exploited to aid in the development of more targeted therapeutics.[12-13] Specifically, studies have also demonstrated that for the MDA-MB-231 breast cancer cell line, endocytosis may play a major role in the invasive properties of the cells.[20] Thus, a detailed understanding of the internalization pathway can aid in strategies for systematic modification of nano-drugs.[14-18]

Our research group has developed selective chemotherapeutic nanomaterials, termed nanoGUMBOS, which are derived from a Group of Uniform Materials Based on Organic Salts (GUMBOS). GUMBOS are organic salts comprised of bulky cationic and anionic moieties. Counter-ion variation in these materials leads to tunable properties such as hydrophobicity, making them particularly suitable for several applications.[21] In that regard, evaluation of data from previous studies showed a correlation between hydrophobicity, charge and chemotherapeutic toxicity. This correlation has been attributed to the more negative mitochondrial membrane potential in cancer cells as compared to normal cells. Thus, lipophilic cations display partially selective localization in cancer cell mitochondria due to this phenomeon.[22-23] While data from these studies reflect mitochondrial localization of several cationic compounds with varying hydrophobicity, the tunable properties of GUMBOS provides a strategy for rapidly tuning the hydrophobicity of a single compound.[24]

Based on a previous study from our group, we have shown that tuning the hydrophobicity of GUMBOS derived from rhodamine 6G (R6G), a fluorescent lipophilic cation, followed by production of nanoGUMBOS from such materials, led to selective toxicity towards the MDA-MB-231 cancer cell line over normal breast cells. This property directly contrasted the

nonselective behavior of the parent dye, rhodamine 6G chloride ([R6G][Cl]).[24] In addition to seletive chemotheraptuic behavior, nanoGUMBOS provide other distinct advantages such as simple synthesis and the ability to serve as a carrier-free therapeutic nanodrug rather than a nanocarrier.[25-26] Furthermore, these R6G nanoGUMBOS displayed dose-dependent toxicity towards multiple breast cancer cell lines, with the highest therapeutic efficacy observed for the MDA-MB-231 cancer cell line. Similar to the parent dye [R6G][Cl], mitochondrial localization of R6G nanoGUMBOS led to mitochondrial dysfunction in cancer cells. Magut, *et al.* attributed this selective chemotherapeutic toxicity of R6G nanoGUMBOS to their enhanced cellular uptake in cancer cells as compared to normal cells.[24] However, while the results presented in Magut *et al.* validate this initial hypothesis, these studies overlooked the nontoxic behavior of internalized R6G nanoGUMBOS in normal cells. Thus, a detailed investigation of the cellular uptake pathway of R6G nanoGUMBOS is critical to further elucidate the mechanism of selective chemotherapeutic behavior of nanoGUMBOS.

Herein, the pinocytic internalization of the most hydrophobic nanoGUMBOS from our previous studies, rhodamine 6G bis(trifuoroethylsulfonyl) imide ([R6G][BETI]), is examined using breast cancer (MDA-MB-231) and normal breast (HMEC) cell lines. In these studies, the internalization pathway of [R6G][BETI] nanoGUMBOS was investigated through assessment of cellular uptake and toxicity in the presence and absence of different pinocytosis inhibitors. Subsequently, toxicity was also evaluated in the presence of lysosomal inhibitors to assess the effects of an acidic endosomal environment on the cytotoxicity of our nanoGUMBOS. Finally, *in vivo* studies of the [R6G][BETI] nanoGUMBOS were performed in order to evaluate drug efficacy in a murine tumor model.

Methods

Materials. Rhodamine 6G (95%), phosphate buffered saline (10x concentrate, 0.2 μM

filtered), methylene chloride, dimethylsulfoxide, citric acid monohydrate, sodium phosphate dibasic, chlorpromazine (98%), filipin III (85%), 5 n-ethyl-n-isopropyl amiloride, 4-(2-aminoethyl) benzenesulfonyl fluoride hydrochloride and 0.2 μM nylon filters were purchased from Sigma-Aldrich (Milwaukee, WI). MitoTracker and LysoTracker dyes were purchased from Molecular Probes (Eugene, OR). Chloroquine hydrochloride was purchased from InvivoGen (San Diego, CA). Lithium bis (perfluoroethylsulfonyl) imide was obtained from Dr. Gary Baker (Oak Ridge National Laboratory, Oak Ridge, TN). Triply deionized water was obtained from an Aires High Purity Water System (Port Allen, LA). The cell viability MTT (3-[4,5-Dimethylthiazol-2-yl]-2, 5-diphenyltetrazolium bromide) assay was purchased from Promega Corporation (Madison, WI). TEM grids were purchased from Ted Pella (Redding, CA).

Synthesis of GUMBOS. Rhodamine 6G GUMBOS were prepared using a two-phase ion exchange method modified from literature.[24] Briefly, Rhodamine 6G chloride was dissolved in dichloromethane (DCM) and mixed with lithium bis(perfluoroethylsulonyl) imide (BETI) dissolved in water in a 1:1 mole ratio and 2:1 volume ratio. The two-phase mixture was allowed to stir for 24 h at room temperature. After 24 h of stirring, deionized water was then used to wash the bottom DCM layer to remove sodium/lithium chloride by-product. The water layer was then removed and the sample was placed for rotor-evaporation to remove the DCM layer and further freeze-dried to remove trace amounts of water.

Synthesis and characterization of nanoGUMBOS. Briefly, a 50 mM DMSO solution of GUMBOS was rapidly precipitated in cell media (DMEM containing 10% FBS) such that the percentage of DMSO/cell media was 2% to form a 1 mM solution of nanoGUMBOS. NanoGUMBOS were then left to age for 30 minutes. Subsequently, nanoGUMBOS were diluted in cell media to a working concentration of 100 μM for characterization and cell studies. TEM

grids were spotted using 3 μL of nanoGUMBOS solution for characterization. TEM micrographs were obtained using an LVEM5 transmission electron microscope (Delong America, Montreal, Canada). Dynamic light scattering (DLS) studies were performed with a Zetasizer Nanoseries Nano ZS (Malvern Instruments, Worcestershire, UK) instrument. Size analyses of the TEM images were performed using Image J processing. Nanoparticles images were obtained from several sections of the TEM grid and Image J processing was used to size approximately 200 representative nanoparticles. The reported sizes represent the average of these 200 particles with the respective standard deviations.

Cell culture. *In vitro* experiments were performed using normal human breast epithelial cells (HMEC), and hormone-independent human breast adenocarcinoma cells (MDA-MB-231) obtained from the American Tissue Culture Collection (ATCC, Manassas, VA) and maintained in culture according to the recommendations of the supplier. HMEC cells were cultured in Lonza Mammary Epithelial Growth Medium with Lonza MGEM Bullet Kit. MDA-MB-231 cells were cultured in Leibovitz's L-15 Medium containing 10% fetal bovine serum FBS.

Determination of active transport internalization. To assess the use of an energy-dependent mechanism of internalization, the parent dye [R6G][Cl] and [R6G][BETI] nanoGUMBOS were incubated at low temperature (4°C)**.** Briefly, 10,000 MDA-MB-231 breast cancer cells were plated on a 25 mm glass bottom petri dish (10 mm micro cell; Ashland, MA, USA). Subsequently, cells were pre-incubated at 4°C for 30 min, followed by incubation of 25 nM of either [R6G][BETI] nanoGUMBOS or [R6G][Cl] for 30 min. Cells were then washed with phosphate buffered saline and then imaged using a Leica DM RXA2 fluorescence microscope.

Evaluation of endocytic uptake. In brief, approximately 10, 000 MDA-MB-231 breast

cancer or HMEC normal breast epithelial cells were plated on a 25 mm glass bottom petri dish (10 mm micro cell; Ashland, MA, USA) in 3 mL of cell media and incubated at 37 °C for 24 h. After 24 h, cell media were replaced with media containing 7 μg/mL, 3 μg/mL or 2.9 μM of chlorpromazine, Filipin III, and amiloride inhibitor respectively, and cells were then incubated for 2 h. For the sucrose and K^+ depletion inhibitor studies, cells were incubated with sucrose supplemented PBS, K^+ Free HEPES buffer, or the respective controls PBS buffer and K^+ Supplemented HEPES buffer for 1 h. After incubation of the inhibitor solution, cells were incubated with 25 nM of either [R6G][BETI] or [R6G][Cl], and then incubated for another 30 min. After the compound incubation, the cells were washed with PBS. Fluorescence images were taken using a 40× dipping objective lens with the TRITC (excitation 535 ± 15 nm and emission 575 ± 15 nm) fluorescence filter on the Leica DM RXA2 fluorescence microscope for the endocytosis studies.

Flow Cytometry Analysis. Briefly, 200,000 MDA-MB-231 breast cancer cells were seeded on a 6 well plate and allowed to grow for 48 hrs. Cells were subsequently treated with 3 μg/mL, 7 μg/mL, and 2.9 μg/mL of filipin III, chlorprozamine, and amiloride respectively for 2 hrs. Cells were then incubated with 500 nm of either [R6G][Cl] or [R6G][BETI] for 30 minutes. Following the 30 minute incubation, cells were washed several times with phosphate buffered saline to wash away any excess dye. Subsequently, cells were trypsinized and centrifuged at 1500 rpm for 8 minutes. The supernatant was removed and the pellet of cells was then suspended in PBS buffer with 2% paraformaldehyde fixating solution prior to flow cytometry analysis.

Kinetic studies of cellular uptake: A 6-well plate was seeded with 100,000 MDA-MB-231 cells/well using RPMI without phenol red and incubated at 37 °C and 5% CO_2 for 24 h. Cells were then incubated with either 12.5 μM [R6G][BETI] nanoGUMBOS or [R6G][Cl] for 0,

15, 30, 60, 120, and 240 minutes. Subsequently, cells were washed with PBS buffer to remove any excess dye. Then, cells were incubated with 3 mL of DMSO overnight for digestion and release of the internal contents. Absorbance measurements were then performed to quantitate amount of internalized [R6G][BETI] nanoGUMBOS or [R6G][Cl]. A calibration curve for each compound, generated using 1, 2, 5, and 10 μM standards, was then used for correlation of the absorbance of the internalized compound relative to the concentration internalized.

Cell viability measurements. In each well of 24-plate, 100,000 MDA-MB-231 cells in 0.5 mL of cell media were seeded and incubated at 37 °C and 5% CO_2 for 24 h. Cells were pre-incubated with 7 μg/mL, 3 μg/mL or 2.9 μg/mL of chlorpromazine, filipin III, and amiloride respectively for 2 h. Subsequently, cells were incubated with a 12.5 μM [R6G][BETI] nanoGUMBOS for 48 hr. Cell viability was assessed using an MTT Assay kit (Promega Corporation, Madison WI, USA). A similar protocol was employed for the lysosomal inhibitors. All results were compared to a control containing no inhibitor.

Study of nanoGUMBOS Dissociation: R6G based nanoGUMBOS were made using the reprecipitation method described above. NanoGUMBOS were then diluted in either a phosphate citric acid buffer at pH 7.4 or pH 4. Buffers were made using triply de-ionized water that was filtered with 0.2 μM nylon filters. DLS and zeta potential measurements were taken for 5 μM nanoGUMBOS using a Malvern Zetasizer instrument.

Evaluation of subcellular localization. 10, 000 MDA-MB-231 breast cancer or HMEC normal breast epithelial cells were plated on a 25 mm glass bottom petri dish (10 mm micro cell; Ashland, MA, USA) in 3 mL of cell media and incubated at 37 °C for 24 h. 1 mM DMSO stock solutions of LysoTracker and MitoTracker were diluted to 15 and 10 nM in cell media respectively. NanoGUMBOS were diluted to 25 nM working concentration in cell media.

Subsequently, the 15 nM LysoTracker solution was incubated with the cells for 20 min. This solution was then removed, and cells were washed once with PBS buffer to remove any excess dye not taken up by cells. A 10 nM MitoTracker solution was then incubated with the cells for 20 min. This solution was then removed, and cells were washed once with PBS buffer to remove any excess dye not internalized by cells. Finally, the 25 nM nanoGUMBOS solution was incubated with the cells for 30 min. This solution was then removed and cells were washed with PBS buffer to remove excess dye. Cell media was replaced with PBS buffer for imaging. Al images were obtained on a Zeiss Observer Z1 Fluorescence microscope using a 63x objective.

***In vivo* studies.** Athymic nude mice were used for *in vivo* studies employing approved IACUC guidelines of Louisiana State University (protocol 14-055) and humane care of animals used in these studies was ensured. A breast cancer xenograft was developed by use of a subcutaneous injection of MDA-MB-231 cancer cells into 15 female athymic nude mice (Crl:NU(NCr)-Foxn1^{nu}) from Charles River. Tumor nodules were allowed to reach approximately 1 cm for 41 days, followed by subsequent injection at the tumor site with PBS buffer, 0.16 mg/kg [R6G][BETI] nanoGUMBOS, or 1.6 mg/kg of [R6G][BETI] nanoGUMBOS on days 41, 42 and 43. The mice were maintained for 56 days and tumor volumes were determined via daily measurements of the smallest (d) and the largest (D) diameters with calipers, and volumes were calculated employing the formula: $V = D \times d^2 \times 0.52$.

Statistical analysis. All experiments were performed in triplicate at least three times. Data are presented as the mean ± standard deviation of the data points. For the cell viability studies, a Student's t-test was used, and for the *in vivo* tumor growth study, a 2-way ANOVA analysis was used with Bonferroni post-test analysis. Statistical calculations were performed using GraphPad Prism 5.0 software (GraphPad Software; La Jolla, CA, USA). Data were

considered statistically significant when $p<0.05$.

Results

NanoGUMBOS Characterization. [R6G][BETI] GUMBOS were synthesized using an ion-exchange reaction as reported by Magut *et al*. (Supplemental Figure S1).[24] Subsequently, [R6G][BETI] nanoGUMBOS were synthesized using a reprecipitation method as outlined in the methods section. Endocytic uptake of nanomaterials can occur via caveolin-mediated endocytosis, clathrin-mediated endocytosis, or micropinocytosis depending upon nanoparticle size, and shape. Thus, characterization of nanomaterials is essential to understanding the mechanism of cellular uptake. In this study, transmission electron microscopy (TEM) was used to characterize the size and shape of [R6G][BETI] nanoGUMBOS. The TEM images presented in Supplemental Figure S2 display spherical nanoparticles with sizes around 100 nm as depicted in the size distribution histogram. A polydispersity index of around 0.2 was observed using dynamic light scattering analysis, indicating relatively monodisperse nanoparticles. Previous literature has demonstrated that spherical nanomaterials with sizes around 100 nm are optimal for a clathrin-mediated pathway [10]. Therefore, we anticipate that uptake of our [R6G][BETI] nanoGUMBOS should occur via clathrin-mediated endocytosis.

Endocytosis studies. Following TEM characterization, the internalization mechanism of the nanoGUMBOS was examined using fluorescence microscopy and cell viability assays. Firstly, cellular uptake of the [R6G][BETI] nanoGUMBOS and [R6G][Cl] in MDA-MB-231 cancer cells was evaluated at cold temperature (4° C) and a control temperature at 37° C using fluorescence microscopy. Literature has shown that cold temperatures disrupt internalization pathways dependent upon energy, such as endocytosis.[27] As shown in Figure 1, incubation at low temperatures resulted in diminished fluorescence intensity for [R6G][BETI] nanoGUMBOS,

demonstrating the use of an energy-dependent pathway of internalization such as endocytosis to internalize in cancer cells. In contrast, the fluorescence intensity of [R6G][Cl] was unaffected at low temperatures indicating that this compound employs an independent energy pathway of internalization such as diffusion.

As endocytosis is a major energy-dependent pathway for internalization of nanoparticles, the role of endocytosis in the internalization of [R6G][BETI] nanoGUMBOS was studied using several inhibitors in conjunction with fluorescence microscopy. Three pinocytosis inhibitors [Filipin III, chlorpromazine hydrochloride, and 5 N-ethyl-N-isopropyl amiloride (amiloride)] were used to block caveolin-mediated endocytosis, clathrin-mediated endocytosis, and micropinocytosis respectively.[28-30] As seen in Figure 2A, a significant reduction in fluorescence intensity was observed for [R6G][BETI] nanoGUMBOS in the presence of chlorpromazine and filipin III in MDA-MB-231 cancer cells. While diminished fluorescence intensity was also observed in the presence of Filipin III, an inhibitor of caveolin-mediated endocytosis, this result can be attributed to lack of specificity of the inhibitor. Dutta et al. reported that Filipin III could also block clathrin-mediated endocytosis in addition to caveolin mediated pathways.[31] Thus, while the role of caveolin pathways on the internalization of nanoGUMBOS is still uncertain, these studies demonstrate that studies that clathrin-mediated endocytosis plays a major role in nanoGUMBOS uptake. As shown in Figure 2A, the fluorescence intensity of [R6G][Cl] remains unaffected in the presence of pinocytic inhibitors in MDA-MB-231 breast cancer cells indicating internalization independent of endocytosis in cancer cells. Examination of these studies in HMEC normal breast epithelial cells is presented in Figure 2B. Interestingly, little or no change was observed in the fluorescence intensity of the parent dye or [R6G][BETI] nanoGUMBOS in the presence of these pinocytic inhibitors. Thus, these results indicate endocytosis-dependent

internalization of [R6G][BETI] nanoGUMBOS in cancer cells and endocytosis-independent internalization in normal cells.

These results are consistent with the mean fluorescence intensities quantitated from flow cytometry analysis and are reported in 2C. While a slight reduction is observed in the presence of chlorpromazine for [R6G][Cl], this reduction is much less as compared to that of the nanoGUMBOS. Furthermore, this slight reduction is consistent with the slight increase in cell viability that is observed with the parent dye in the presence of chlorpromazine. These results suggest a minor use of clathrin mediated endocytosis by the parent dye. However, the strong fluorescence intensity of parent dye within the cell in the presence of the chlorpromazine inhibitor suggests the use of another internalization pathway as the primary pathway of internalization. As shown in Figure 1, a strong fluorescence is also observed for [R6G][Cl] when incubated at low temperature (4 °C). This suggests that this dye most likely uses a passive mode of internalization since active transport mechanisms are hindered at low temperature. Thus, while [R6G][Cl] may employ clathrin mediated endocytosis as a minor pathway of internalization, these results suggest that the dye can still internalize into the cell when endocytic internalization is disrupted. In contrast to the parent dye, the more significant reduction in fluorescence intensity for [R6G][BETI] nanoGUMBOS in the presence of chlorpromazine suggests the primary use of clathrin mediated endocytosis for nanoGUMBOS.

To further confirm our observations, fluorescence microscopy of the compounds was performed in the presence of a hypertonic solution (sucrose supplemented PBS buffer) and a potassium (K^+) depletion solution (K^+ free HEPES buffer). Previous studies have shown that these solutions can disrupt the formation of clathrin-coated pits that form during clathrin-mediated endocytosis. [27, 32] As depicted in Figure 3A, a significant reduction in fluorescence

intensity was observed for [R6G][BETI] nanoGUMBOS in the presence of both the hypertonic and K^+ depletion conditions in examined cancer cells. These results suggest that disruption of the clathrin-coated pit formation by the employed inhibitor solutions resulted in inhibited nanoparticle internalization, thus confirming our earlier results that [R6G][BETI] nanoGUMBOS primarily use clathrin-mediated endocytosis for internalization in cancer cells. In contrast, no change in the fluorescence intensity was observed for [R6G][Cl] as in the presence of the inhibitors. Thus, these results support the conclusion that [R6G][Cl] internalizes via an endocytosis-independent pathway. Furthermore, the fluorescence intensity of both compounds remained unaffected in the presence of these pinocytosis inhibitors in normal breast cells (Figure 3B). These results corroborate the previous microscopy results that show while [R6G][BETI] nanoGUMBOS are internalized via an endocytic pathway in cancer cells, internalization of [R6G][BETI] into normal breast cells is independent of endocytosis.

In order to further understand the uptake mechanism for the [R6G][BETI] nanoGUMBOS and [R6G][Cl], cell viability was examined at the IC_{50} concentration (12.5 μM) of the former in conjunction with pinocytosis inhibitors in MDA-MB-231 breast cancer cells and HMEC breast normal cells. Our previous investigations have demonstrated toxicity of [R6G][BETI] nanoGUMBOS towards MDA-MB-231 breast cancer cells. Therefore, an increase in cell viability of the compounds in the presence of pinocytosis inhibitors could signify the pathway for cellular uptake. Samples containing only inhibitor and no drug were used as a control to ensure a nontoxic concentration of inhibitor. In the presence of chlorpromazine, a substantial increase in cell viability was observed with [R6G][BETI] nanoGUMBOS (Figure 4A). When examining the cytotoxic effect of the original dye (i.e., [R6G][Cl]), a statistically significant increase was seen in cell viability in the presence of chlorpromazine as well.

However, this increase is relatively small as compared to our [R6G][BETI] nanoGUMBOS. No increase in cell viability was observed with filipin III or amiloride inhibitors, suggesting that [R6G][BETI] nanoGUMBOS are not internalized using these pathways. Examination of these studies in HMEC normal cells shows no change in cell viability of the [R6G][BETI] nanoGUMBOS in the presence of pinocytosis inhibitors signifying internalization independent of endocytosis (Figure 4B). These results indicate that clathrin-mediated endocytosis is the major internalization mechanism for the [R6G][BETI] nanoGUMBOS in cancer cells while internalization in normal cells is independent of endocytosis. Further supporting our findings, the saturation results obtained with cellular uptake of [R6G][BETI] nanoGUMBOS in MDA-MB-231 breast cancer cells after 100 min (Supplemental Figure S3), in contrast to the linear cellular uptake of the parent dye, [R6G][Cl], are also consistent with other studies of the kinetics of endocytic internalization.[33,34]

Lysosomal inhibitors. Literature reports clathrin-mediated endocytosis requires the nanoparticle to pass through the acidic lysosome before release into the target organelle.[35] Thus, cell viability studies were examined in the presence of lysosomotrophic inhibitors to examine the role of lysosomal acidification or lysosome enzymes, such as proteases, on the [R6G][BETI] nanoGUMBOS toxicity. The cell viability studies show that the toxicity of these nanoGUMBOS towards MDA-MB-231 cancer cells was significantly reduced in the presence of the inhibitor chloroquine, while the toxicity is unaffected in the presence of the protease inhibitor 4-(2-aminoethyl) benzenesulfonyl fluoride hydrochloride (Figure 5). Similar results were observed with other protease inhibitors (Supplemental Figure S4**)**. In contrast, the toxicity of [R6G][Cl] was unaffected by either lysosomotropic inhibitor. TEM images presented in Figure 6 show loss of nanoparticle shape at lysosomal pH, suggesting dissociation of the [R6G][BETI]

nanoGUMBOS within the acidic lysosome. Evaluation of other pH environments is presented in Supplemental Figure S5. In addition, DLS results Figure 6, indicate a loss of signal at acidic pH, further confirming the results from TEM. These results suggest that our nanoGUMBOS dissociate in cancer cells through lysosomal acidification following endocytic uptake. Analysis of zeta potential suggests a relatively stable nanoparticle suspension at physiological pH and rapid precipitation of at lysosomal pH (Supplemental Table S1). Subcellular localization studies presented in Supplemental Figure S6 demonstrated significant co-localization of [R6G][BETI] nanoGUMBOS with the Mitotracker dye and minimal co-localization with the Lysotracker dye in both cancer and normal cells, similar to the parent dye [R6G][Cl]. This result implies that following endocytic uptake in cancer cells, the dissociated nanoGUMBOS are released from the endosome and subsequently target the mitochondria.

***In vivo* examination.** Following our examination of the *in vitro* mechanism of selectivity, we pursued *in vivo* studies of these [R6G][BETI] nanoGUMBOS to determine if selectivity and therapeutic properties would be maintained. For our examination of tumor reduction, MDA-MB-231 cancer cells were used to produce a tumor on the right flank of 12 athymic nude mice. The mice were randomized into three groups four mice per group. One group was injected at the tumor site with phosphate-buffered saline solution (PBS buffer), a second group was treated with 0.16 mg/kg [R6G][BETI] nanoGUMBOS, and a third group was treated with 1.6 mg/kg of [R6G]BETI] nanoGUMBOS, on days 41, 42 and 53. The volumes of the tumors (Figure 7) in these mice were monitored before and after treatment with [R6G][BETI]. As shown in Figure 7, control mice treated with only saline solution showed a continued increase in tumor volume (Figure 7). However, mice injected with treated with either 0.16 mg/kg or 1.6 mg/kg of [R6G][BETI] showed a 50% reduction in the tumor volume. These

studies showed that [R6G][BETI] nanoGUMBOS not only inhibit tumor growth but also reduce tumor volume in mice by almost 50%.

Discussion

Mechanism of selective toxicity. Results from the endocytosis studies indicate uptake of [R6G][BETI] nanoGUMBOS occurs primarily via clathrin-mediated endocytosis in cancer cells, and that it is independent of endocytosis in normal cells. The decreased toxicity of nanoGUMBOS in the presence of lysosomal acidification inhibitor chloroquine implies that the acidic lysosomal environment activates toxicity of the nanoGUMBOS during endocytic uptake in cancer cells. Characterization of nanoGUMBOS at varying values of pH suggests that activation of toxicity can be attributed to dissociation of the nanoGUMBOS at the acidic lysosomal pH (4.3).[35] In contrast, due to the endocytosis-independent internalization of the nanoGUMBOS in normal cells, the lysosome is bypassed. Therefore, the nanoparticles do not dissociate under these conditions, resulting in their nontoxic behavior in normal cells. In the case of the parent dye [R6G][Cl], no dissociation is needed to activate the toxicity due to its high solubility in aqueous media, resulting in its inherent toxicity towards both cancer and normal cells.

Reduction in tumor volume: *In-vivo* investigations of the R6G nanoGUMBOS indicated retention of the therapeutic properties of the nanoGUMBOS within the athymic nude mouse model examined. These studies suggest that [R6G][BETI] nanoGUMBOS not only inhibit tumor growth but also reduce tumor volume in mice by almost 50%. Similarities in therapeutic efficacy of the nanoGUMBOS with the two different doses could be attributed to saturation of the drug within the tumor at the lower dose. Furthermore, lack of further decrease in tumor volume can be attributed to the formation of necrotic tissue at the surface of the tumor; thus, preventing penetration of the nanoGUMBOS deeper in the tumor. [36]

The studies reported here demonstrate the critical role of endocytosis in both the internalization and selectivity mechanisms of R6G nanoGUMBOS, and reveal promising *in vivo* therapeutic properties of these materials. We found that endocytic internalization of these nanoGUMBOS in cancer cells resulted in dissociation of these nanomaterials within the acidic endosome, ultimately activating their chemotherapeutic toxicity. In contrast, because the R6G nanoGUMBOS employed endocytosis-independent internalization in normal cells, the nanoparticles were not dissociated under such conditions, resulting in their nontoxic behavior in normal cells. Investigation of the therapeutic efficacy of these nanomaterials using a mouse xenograft model demonstrated retention of their therapeutic properties *in vivo*. Moreover, these *in vitro* and *in vivo* studies have enhanced our understanding of R6G nanoGUMBOS and confirmed the potential of these novel compounds and similar strategies for chemotherapeutic applications. Future studies will focus on determining their pharmacokinetic and pharmacodynamic properties *in vivo.*

Acknowledgements

This material is based upon work supported by the National Science Foundation under Grants CHE-1307611 and CHE-1508726. Any opinions, findings, and conclusions or recommendations expressed in this material are those of the author(s) and do not necessarily reflect the views of the National Science Foundation. We thank Dr. Rafael E. Luna, Executive Director of the National Research Mentoring Network (Boston College), for discussions regarding aspects of scientific writing for this manuscript. The use of LSU Shared Instrumentation Facility is also acknowledged.

Conflict of Interest

The authors declare no potential conflicts of interest.

Supplemental Information.

Scheme for the synthesis of [R6G][BETI] GUMBOS, TEM characterization of R6G nanoGUMBOS, kinetic studies for internalization, toxicity of nanoGUMBOS and [R6G][Cl] in the presence and absence of protease inhibitors, TEM images of nanoGUMBOS at various pH values, zeta potential of nanoGUMBOS at lysosomal and physiological values of pH, and mitochondrial localization of images

References

1. Siegel, R. L.; Miller, K. D.; Jemal, A., Cancer statistics, 2015. *CA: A Cancer Journal for Clinicians* **2015,** *65* (1), 5-29.
2. de la Zerda, A.; Gambhir, S. S., Drug delivery: Keeping tabs on nanocarriers. *Nat Nano* **2007,** *2* (12), 745-746.
3. Wicki, A.; Witzigmann, D.; Balasubramanian, V.; Huwyler, J., Nanomedicine in cancer therapy: Challenges, opportunities, and clinical applications. *Journal of Controlled Release* **2015,** *200*, 138-157.
4. Peer, D.; Karp, J. M.; Hong, S.; Farokhzad, O. C.; Margalit, R.; Langer, R., Nanocarriers as an emerging platform for cancer therapy. *Nat Nano* **2007,** *2* (12), 751-760.
5. Pérez-Herrero, E.; Fernández-Medarde, A., Advanced targeted therapies in cancer: Drug nanocarriers, the future of chemotherapy. *European Journal of Pharmaceutics and Biopharmaceutics* **2015,** *93*, 52-79.
6. Gao, J.; Xu, B., Applications of nanomaterials inside cells. *Nano Today* **2009,** *4* (1), 37-51.
7. Krishnamurthy, S.; Vaiyapuri, R.; Zhang, L.; Chan, J. M., Lipid-coated polymeric nanoparticles for cancer drug delivery. *Biomaterials Science* **2015,** *3* (7), 923-936.
8. Mura, S.; Nicolas, J.; Couvreur, P., Stimuli-responsive nanocarriers for drug delivery. *Nat Mater* **2013,** *12* (11), 991-1003.
9. Sun, T.; Zhang, Y. S.; Pang, B.; Hyun, D. C.; Yang, M.; Xia, Y., Engineered Nanoparticles for Drug Delivery in Cancer Therapy. *Angewandte Chemie International Edition* **2014,** *53* (46), 12320-12364.
10. Sahay, G.; Alakhova, D. Y.; Kabanov, A. V., Endocytosis of nanomedicines. *Journal of Controlled Release* **2010,** *145* (3), 182-195.
11. Champion, J. A.; Walker, A.; Mitragotri, S., Role of Particle Size in Phagocytosis of Polymeric Microspheres. *Pharmaceutical research* **2008,** *25* (8), 1815-1821.
12. Floyd, S.; De Camilli, P., Endocytosis proteins and cancer: a potential link? *Trends in Cell Biology* **1998,** *8* (8), 299-301.

13. Jones, A. T.; Gumbleton, M.; Duncan, R., Understanding endocytic pathways and intracellular trafficking: a prerequisite for effective design of advanced drug delivery systems. *Advanced Drug Delivery Reviews* **2003,** *55* (11), 1353-1357.
14. Iversen, T.-G.; Skotland, T.; Sandvig, K., Endocytosis and intracellular transport of nanoparticles: Present knowledge and need for future studies. *Nano Today* **2011,** *6* (2), 176-185.
15. Bareford, L. M.; Swaan, P. W., Endocytic Mechanisms for Targeted Drug Delivery. *Advanced drug delivery reviews* **2007,** *59* (8), 748-758.
16. Sahay, G.; Kim, J. O.; Kabanov, A. V.; Bronich, T. K., The exploitation of differential endocytic pathways in normal and tumor cells in the selective targeting of nanoparticulate chemotherapeutic agents. *Biomaterials* **2010,** *31* (5), 923-933.
17. Akinc, A.; Battaglia, G., Exploiting endocytosis for nanomedicines. *Cold Spring Harbor perspectives in biology* **2013,** *5* (11), a016980.
18. Mellman, I.; Yarden, Y., Endocytosis and Cancer. *Cold Spring Harbor Perspectives in Biology* **2013,** *5* (12), a016949.
19. Huang, Y.; He, L.; Liu, W.; Fan, C.; Zheng, W.; Wong, Y.-S.; Chen, T., Selective cellular uptake and induction of apoptosis of cancer-targeted selenium nanoparticles. *Biomaterials* **2013,** *34* (29), 7106-7116.
20. Bodenstine, T. M.; Seftor, R. E. B.; Seftor, E. A.; Khalkhali-Ellis, Z.; Samii, N. A.; Monarrez, J. C.; Chandler, G. S.; Pemberton, P. A.; Hendrix, M. J. C., Internalization by Multiple Endocytic Pathways and Lysosomal Processing Impact Maspin-based Therapeutics. *Molecular cancer research : MCR* **2014,** *12* (10), 1480-1491.
21. Warner, I. M.; El-Zahab, B.; Siraj, N., Perspectives on Moving Ionic Liquid Chemistry into the Solid Phase. *Analytical Chemistry* **2014,** *86* (15), 7184-7191.
22. Modica-Napolitano, J. S.; Aprille, J. R., Delocalized lipophilic cations selectively target the mitochondria of carcinoma cells. *Advanced Drug Delivery Reviews* **2001,** *49* (1–2), 63-70.
23. Belostotsky, I.; da Silva, S. M.; Paez, M. G.; Indig, G. L., Mitochondrial targeting for photochemotherapy. Can selective tumor cell killing be predicted based on n-octanol/water distribution coefficients? *Biotechnic & Histochemistry* **2011,** *86* (5), 302-314.
24. Magut, P. K.; Das, S.; Fernand, V. E.; Losso, J.; McDonough, K.; Naylor, B. M.; Aggarwal, S.; Warner, I. M., Tunable cytotoxicity of rhodamine 6G via anion variations. *Journal of the American Chemical Society* **2013,** *135* (42), 15873-9.
25. Farokhzad, O. C.; Langer, R., Nanomedicine: Developing smarter therapeutic and diagnostic modalities. *Advanced Drug Delivery Reviews* **2006,** *58* (14), 1456-1459.
26. Kumari, A.; Yadav, S. K.; Yadav, S. C., Biodegradable polymeric nanoparticles based drug delivery systems. *Colloids and Surfaces B: Biointerfaces* **2010,** *75* (1), 1-18.
27. Hu, Z.; Pan, Y.; Wang, J.; Chen, J.; Li, J.; Ren, L., Meso-tetra (carboxyphenyl) porphyrin (TCPP) nanoparticles were internalized by SW480 cells by a clathrin-mediated endocytosis pathway to induce high photocytotoxicity. *Biomedicine & Pharmacotherapy* **2009,** *63* (2), 155-164.
28. Rejman, J.; Bragonzi, A.; Conese, M., Role of clathrin- and caveolae-mediated endocytosis in gene transfer mediated by lipo- and polyplexes. *Molecular therapy : the journal of the American Society of Gene Therapy* **2005,** *12* (3), 468-74.
29. Watson, P.; Jones, A. T.; Stephens, D. J., Intracellular trafficking pathways and drug delivery: fluorescence imaging of living and fixed cells. *Adv Drug Deliv Rev* **2005,** *57* (1), 43-61.
30. Schnitzer, J. E.; Oh, P.; Pinney, E.; Allard, J., Filipin-sensitive caveolae-mediated transport in endothelium: reduced transcytosis, scavenger endocytosis, and capillary permeability of select macromolecules. *The Journal of cell biology* **1994,** *127* (5), 1217-1232.
31. Dutta, D.; Donaldson, J. G., Search for inhibitors of endocytosis: Intended specificity and unintended consequences. *Cellular Logistics* **2012,** *2* (4), 203-208.

32. Hansen, S.; Sandvig, K.; van Deurs, B., *Clathrin and HA2 adaptors: Effects of potassium depletion, hypertonic medium, and cytosol acidification*. 1993; Vol. 121, p 61-72.
33. Zhang, D.; Lee, H.-F.; Pettit, S. C.; Zaro, J. L.; Huang, N.; Shen, W.-C., Characterization of transferrin receptor-mediated endocytosis and cellular iron delivery of recombinant human serum transferrin from rice (Oryza sativaL.). *BMC Biotechnology* **2012,** *12* (1), 92.
34. Gáborik, Z.; Szaszák, M.; Szidonya, L.; Balla, B.; Paku, S.; Catt, K. J.; Clark, A. J. L.; Hunyady, L., β-Arrestin- and Dynamin-Dependent Endocytosis of the AT₁ Angiotensin Receptor. *Molecular Pharmacology* **2001,** *59* (2), 239-247.
35. Mindell, J. A., Lysosomal Acidification Mechanisms. *Annual Review of Physiology* **2012,** *74* (1), 69-86.
36. Minchinton, A. I.; Tannock, I. F., Drug penetration in solid tumours. *Nat Rev Cancer* **2006,** *6* (8), 583-592.

Figures:

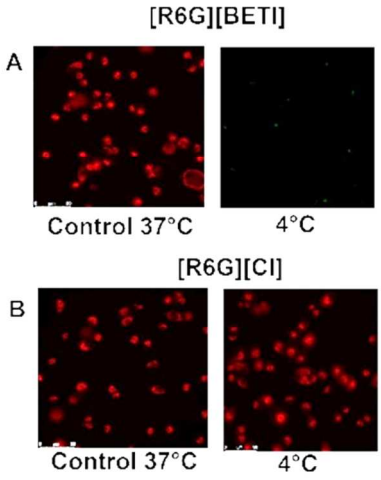

Figure 1. (A) 25 nM [R6G][BETI] incubated at 37°C and 4 °C in MDA-MB-231 cancer cells **(B)** 25 nM [R6G][Cl] incubated at 37°C and 4 °C in MDA-MB-231 cancer cells.

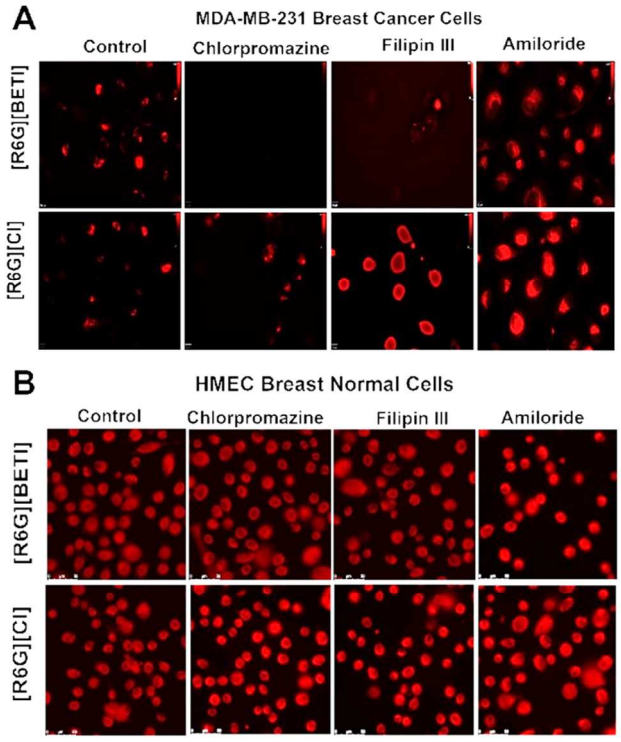

C. Mean fluorescence intensity of MDA-MB-231 breast cancer cells incubated with [R6G][BETI] and [R6G][Cl] in the presence of various endocytosis inhibitors.

Compound	Mean Fluorescence Intensity
[R6G][BETI] Control	511.5 ± 81.1
[R6G][BETI] Chlorpromazine	4.3 ± 0.8
[R6G][BETI] Filipin	18.5 ± 0.4
[R6G][BETI] Amiloride	338.0 ± 66.5
[R6G][Cl] Control	600.3 ± 104.0
[R6G][Cl] Chlorpromazine	243.9 ± 92.6
[R6G][Cl] Filipin	445.4 ±38.1

Figure 2. [R6G][BETI] or [R6G][Cl] incubated in 3 µg/mL, 7 µg/mL, and 2.9 µg/mL of filipin III, chlorprozamine, and amiloride in **(A)** MDA-MB-231 breast cancer cells. **(B)** HMEC breast epithelial normal cells and **(C)** Mean fluorescence intensities from fow cytometry analysis of MDA-MB-231 breat cancer cells incubated with either [R6G][BETI] or [R6G][Cl] in the presence of the endocytosis inhibitors.

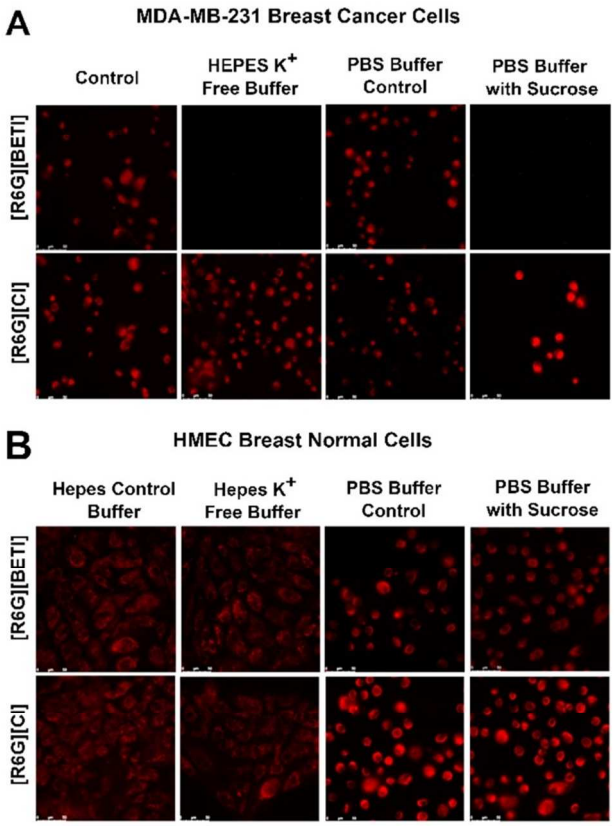

Figure 3. [R6G][BETI] and [R6G][Cl]incubated in the presence of HEPES buffer with and without KCl and PBS Buffer with and without sucrose in **(A)** MDA-MB-231 breast cancer cells and **(B)** HMEC breast epithelial cells.

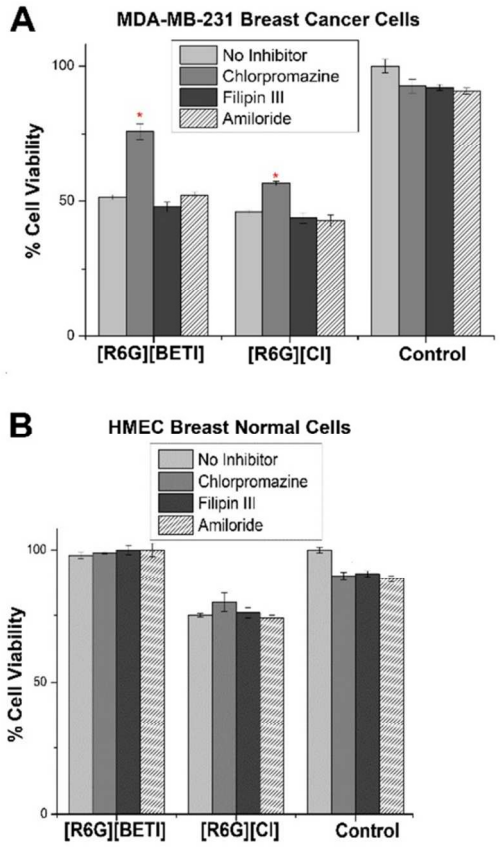

Figure 4. Cell viability of R6G compounds in the presence of 3 µg/mL, 7 µg/mL and 2.9 µg/mL of filipin III, chlorpromazine and amiloride respectively in **(A)** MDA-MB-231 breast cancer cells and **(B)** HMEC breast epithelial normal cells. The cell viability results were compared using a Student's t-test; the differences were considered statistically significant if $p \leq 0.05$ (*).

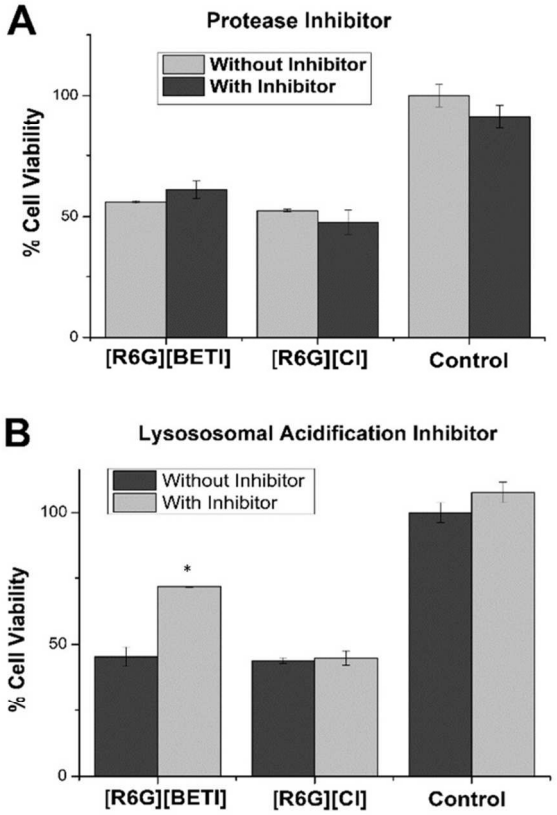

Figure 5. Cell viability of [R6G][BETI] nanoGUMBOS and [R6G][Cl] in the presence of **(A)** 0.5 mM 4-(2-aminoethyl)benzenesulfonyl fluoride hydrochloride (AEBSF Inhibitor) to block serine proteases and **(B)** 100 µM of chloroquine to prevent lysosomal acidification. The cell viability results were compared using a Student's t-test; the differences were considered statistically significant if $p = 0.05$ (*)

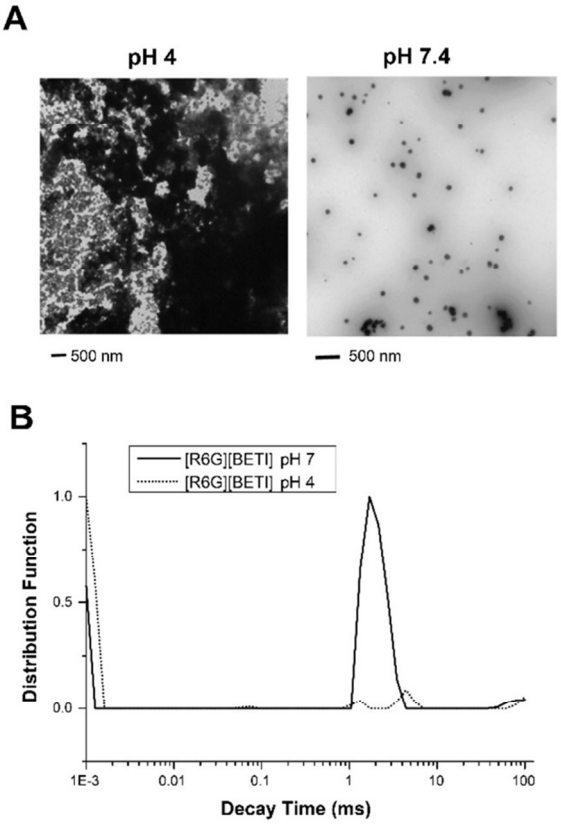

Figure 6. (A) TEM characterization of nanoGUMBOS at lysosomal and physiological pH and **(B)** Plot of particle size distribution function vs. decay time at physiological and lysosomal pH.

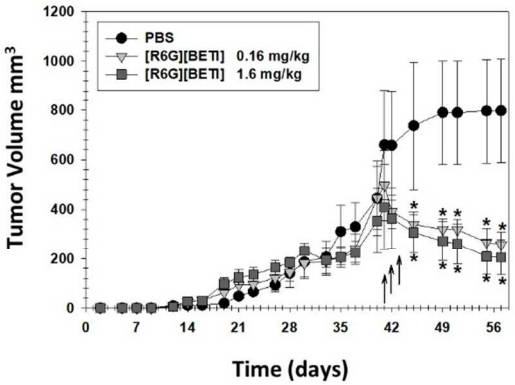

Figure 7. In-vivo tumor reduction using 0.16 and 1.6 mg/kg of [R6G][BETI] as compared to a saline control. Tumor measurements were compared by a two-way ANOVA and a Bonferroni post-test; the differences were considered statistically significant if p = 0.05 (*). Arrows represent days of injection.